Continuous-wave, all-solid-state, single-frequency 400-mW source at 589 nm based on doubly resonant sum-frequency mixing in a monolithic lithium niobate resonator

Joseph D. Vance, Chiao-Yao She, and Hans Moosmüller

Sum-frequency mixing of two cw single-mode Nd:YAG lasers in a doubly resonant congruent lithium niobate resonator generated two TEM_{00} beams of single-frequency 589-nm radiation. The primary beam had a power of 400 mW and the secondary beam of approximately 15 mW by use of 320 mW of 1319-nm and 660 mW of 1064-nm Nd:YAG radiation incident on the lithium niobate resonator. This corresponds to an optical power conversion efficiency of more than 40%. © 1998 Optical Society of America

OCIS codes: 140.0140, 160.3730, 190.0190, 230.5750, 350.5610.

1. Introduction

Coherent cw light sources in the visible region are important for a number of scientific and technical applications including metrology, remote sensing, biotechnology, communications, and display technology. Recently, frequency-doubled, diode-pumped Nd^{3+} lasers have been established as compact, efficient, all-solid-state sources in the blue, green, and red spectral regions. However, the region between 550 and 650 nm is not covered by these sources. Laser radiation near 620 and 590 nm is required for display technology and medical applications, respectively.[1] In addition, cw single-frequency radiation at the sodium D_2 line (589 nm) is needed for laboratory spectroscopy and atmospheric remote-sensing applications in the mesopause region.[2] Of interest for this application is cw sum-frequency generation because the generated radiation has a narrow bandwidth and can be locked to sub-Doppler features of the sodium D_2 line. Such a system could, for example, replace the single-mode ring dye lasers currently used in narrow-band sodium lidar systems for atmospheric temperature and wind velocity measurements in the mesopause region, making a mobile system feasible.[3,4] The near-Fourier-transform-limited dye amplifiers currently used in these lidar systems require a minimum cw input power of ≈150 mW.

One approach to generate radiation at these wavelengths utilizes cw sum-frequency mixing of the output of two Nd^{3+} lasers. Recently, this approach was used to generate 3.4 mW of single-frequency 589-nm radiation in an external lithium niobate ($LiNbO_3$) crystal without cavity enhancement.[2] Recently, 212 mW of 618-nm radiation was generated by doubly resonant intracavity sum-frequency mixing in a lithium triborate (LiB_3O_5 or LBO) crystal[1] and 2.5 W of 629-nm radiation by an optical parametric oscillator process and sum-frequency generation in a singly resonant discrete external resonator utilizing a dual-grating periodically poled lithium niobate crystal.[5]

In this paper we report efficient doubly resonant sum-frequency generation in an external monolithic $LiNbO_3$ resonator generating more than 400 mW of cw single-frequency 589-nm radiation with more than 40% optical power conversion efficiency in the mixing process. To the best of our knowledge, this represents the highest cw power reported for an all-solid-state system at 589 nm and the highest nondegenerate sum-frequency mixing efficiency reported for cw sources. In addition, the external resonator approach is not plagued by chaotic power oscillations

J. D. Vance and H. Moosmüller are with the Desert Research Institute, University of Nevada System, P.O. Box 60220, Reno, Nevada 89506. C.-Y. She is with the Department of Physics, Colorado State University, Fort Collins, Colorado 80523.

Received 14 October 1997; revised manuscript received 30 March 1998.

0003-6935/98/214891-06$15.00/0

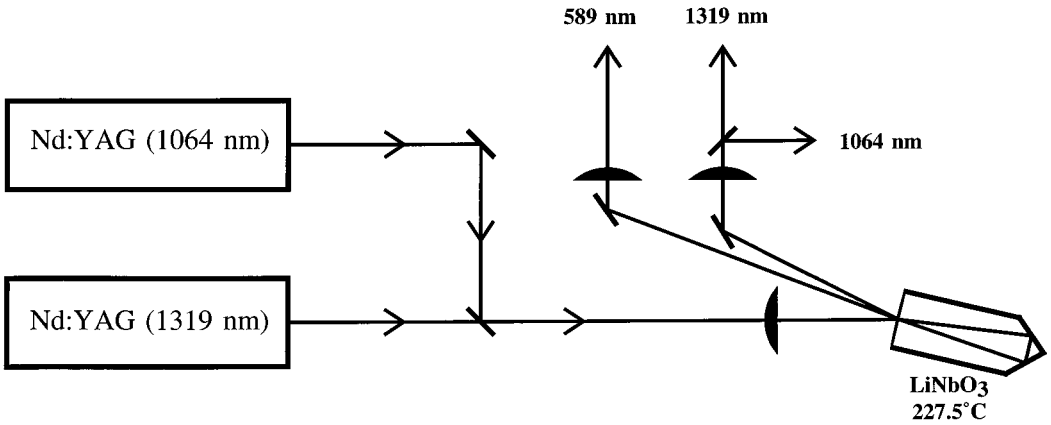

Fig. 1. Schematic diagram of the experimental setup.

(i.e., the green problem) that can be a problem for intracavity approaches.[1,6]

External optical resonators have been used to increase the efficiency of sum-frequency generation for more than three decades.[7] Recent examples include the use of both discrete and monolithic resonators.[8–11] Monolithic resonators are simpler and more stable and have potential for higher resonance enhancement than discrete cavities. The use of a low-loss nonlinear material such as $LiNbO_3$ is essential for efficient sum-frequency generation in a monolithic resonator.

2. Experiment

A schematic of the experimental setup for sum-frequency generation is shown in Fig. 1. Two commercially available Nd:YAG lasers, one emitting 0.7 W near 1064 nm (Lightwave Electronics Model 126-1064-700) and the other one emitting 0.35 W near 1319 nm (Lightwave Electronics Model 126-1319-350) are used as infrared light sources. These lasers are based on a monolithic diode-pumped Nd:YAG ring cavity[12] and incorporate both a relatively fast piezotuning mechanism with a 30-MHz tuning range and a 30-kHz response bandwidth and a slow (1-GHz/s) thermal tuning mechanism with a tuning range of 60 GHz.[13] Their narrow linewidth (5 kHz over 1 ms), TEM_{00} spatial mode, and low amplitude noise (0.05% rms between 10 Hz and 10 MHz) combined with their tunability makes them well suited for the generation of narrow-band, tunable radiation near 589 nm.

After passing through suitably chosen spherical and cylindrical mode-matching lenses, the two vertically (s-) polarized Nd:YAG laser beams are overlapped by use of a long-wave-pass dichroic mirror. The coaxially propagating beams are focused into the monolithic $LiNbO_3$ resonator with an antireflection-coated 250-mm focal length lens resulting in mode-matching efficiencies of approximately 90%. Focal parameters in the resonator are estimated to be z_R = 14 mm for both beams and w_0 = 51 μm for the 1319-nm beam and w_0 = 46 μm for the 1064-nm beam, where z_R is the Rayleigh length and w_0 is the minimum beam radius. The laser powers incident on the resonator were measured to be P_1 = 0.32 W at 1319 nm and P_2 = 0.66 W at 1064 nm. The phase-matching temperature for the sum-frequency mixing process in congruent $LiNbO_3$ was calculated from a dispersion equation[14] to be 227.5 °C, in agreement with our experimental results. The temperature phase-matching bandwidth of congruent lithium niobate is relatively small (i.e., 7 °C mm). The crystal oven used to maintain the resonator temperature at the phase-matching temperature has been described previously.[2]

The monolithic $LiNbO_3$ resonator shown in Fig. 2 is

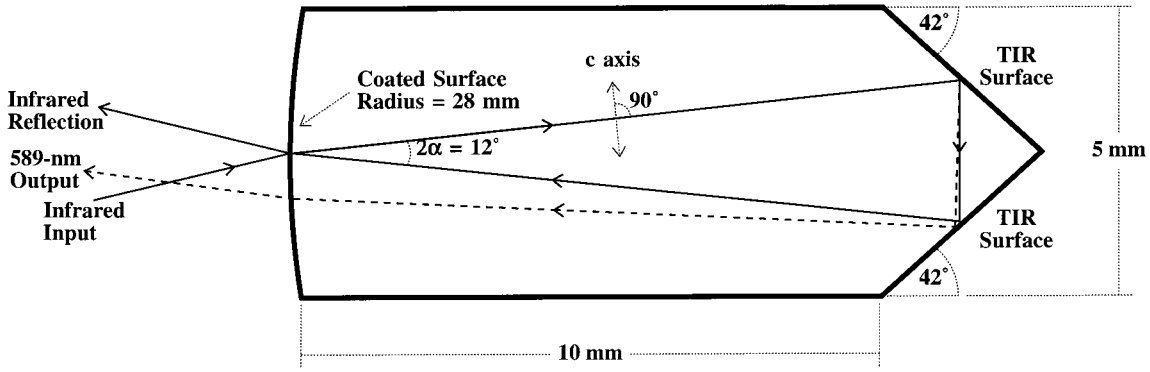

Fig. 2. Monolithic lithium niobate resonator for sum-frequency generation of 589-nm radiation.

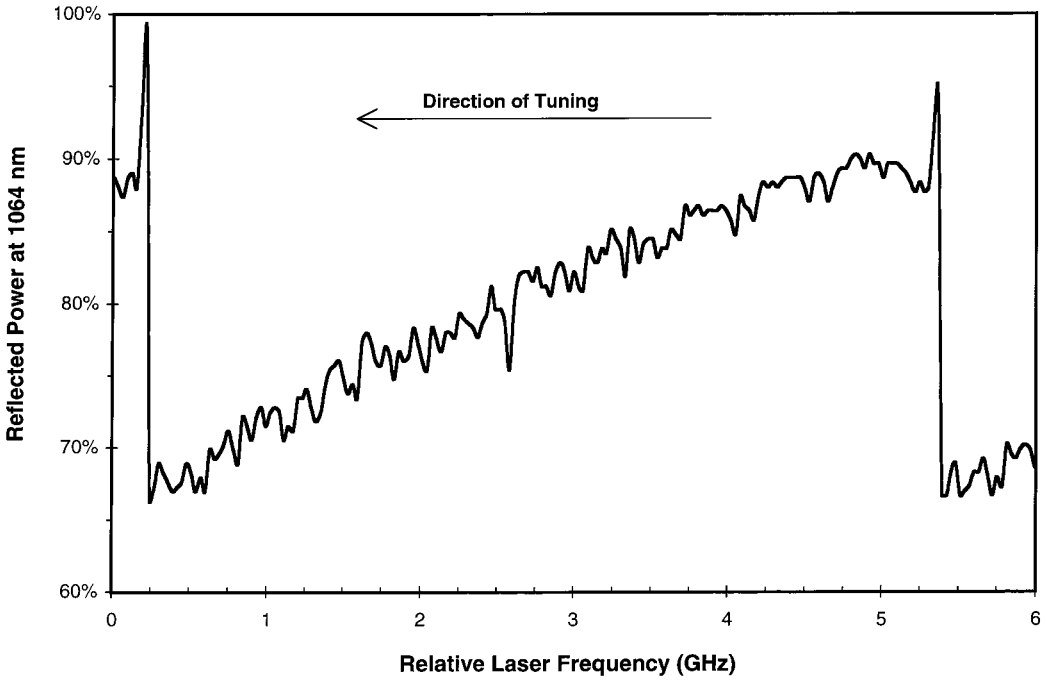

Fig. 3. Fractional power at 1064 nm reflected by the $LiNbO_3$ resonator while tuning the laser toward lower frequency. The resonator mode is clearly asymmetric with the near-linear low-angle ramp being the self-locking region.

similar to a design previously used for second-harmonic generation.[15] It is ≈13 mm long by 5 mm wide by 1.5 mm thick with the *c* axis in the resonator plane at an angle of 84° relative to the 10-mm-long edges. Three surfaces of the $LiNbO_3$ crystal define the optical cavity. A curved surface (r = 28 mm), coated for 97% reflection of *s*-polarized radiation at 1064 and 1319 nm and approximately 96% transmission of *p*-polarized radiation at 589 nm, couples the infrared beams into the cavity and couples out the generated 589-nm beam. Two flat total-internal-reflection (TIR) surfaces complete the ring. The geometric round-trip length L_{rt} of the near-confocal ring resonator is L_{rt} = 25.4 mm, which together with the ordinary refractive indices of congruent $LiNbO_3$ for the *s*-polarized infrared beams [n_o(1064 nm, 227.5 °C) = 2.234, n_o(1319 nm, 227.5 °C) = 2.221][14] results in free spectral ranges of approximately 5.3 GHz. One of the long resonator legs is perpendicular to the crystal's *c* axis, with type I noncritical phase matching at 227.5 °C resulting in sum-frequency generation along this leg over its length L_{pm} = 11.5 mm. The generated *p*-polarized 589-nm beam is purely extraordinary only along the generating leg of the resonator, but after reflection it has both ordinary and extraordinary components. The reflections on the TIR surfaces are therefore bireflections, i.e., the angles of incidence and reflection do not equal each other as shown in Fig. 2. As a consequence, the generated 589-nm beam is coupled out of the resonator at an angle different from that of the reflected infrared beams. In addition, the portion (≈4%) of the 589-nm beam that is reflected on the coated surface undergoes further bireflections on the following round trip (not shown in Fig. 2) and is emitted as a spatially separate second output beam containing somewhat less than 4% of the power of the primary 589-nm output beam.

To achieve power enhancement in the resonator, the laser frequencies must be in coincidence with resonator modes. For the 1319-nm laser this is done by locking its frequency to a resonator mode by modulating the laser frequency and locking the derivative (lock-in amplifier output) of the 1319-nm photodiode signal to its zero crossing with a proportional controller. For the 1064-nm laser, the resonator modes are asymmetrically broadened because of absorption-induced heating in the resonator (this phenomenon also occurs for the 1319-nm laser but to a far lesser extent because of its much lower intracavity power). The additional heating increases the refractive index of $LiNbO_3$, decreasing the frequency of the resonator modes. If the laser frequency is decreased while approaching a resonator mode, the resonator frequency is being continually decreased, i.e., the laser mode keeps pushing the resonator frequency in front of its own frequency until it reaches the resonance peak. An example of the 1064-nm power reflected by the resonator is shown in Fig. 3 with no 1319-nm power incident on the resonator. Impedance matching is relatively poor (power reflectance >65% in Fig. 3) as no 1319-nm radiation is present and no sum-frequency conversion takes place. As the relative laser frequency is decreased from approximately 5 GHz, the 1064-nm field builds up in the resonator, therefore more 1064-nm power is absorbed in the resonator. This results in improved impedance matching, i.e., reduced reflected power and in heating

of the resonator material shifting the resonator mode to a lower frequency. The near-linear ramp of the reflected power as a function of laser frequency is the self-locking range between approximately 5 and 0.25 GHz (Fig. 3) where negative feedback dominates the tuning.[16] Within this range, the thermally induced cavity tuning near resonance leads to self-locking of the resonator mode to the laser frequency, allowing stable, self-locked operation for many hours. When the laser frequency passes the resonance peak at 0.25 GHz, the heating of the lithium niobate is reduced which in turn shifts the resonator mode to a higher frequency and further reduces the heating. This corresponds to a switch from negative feedback in the self-locking region to positive feedback at 0.25 GHz, resulting in a sudden increase in reflected power. Asymmetric mode broadening in a monolithic $LiNbO_3$ resonator has been observed previously,[15] and thermally induced self-locking of a resonator mode and the resulting bistability has been analyzed in some detail for a doubly resonant optical parametric oscillator,[17] for resonator mirror absorption,[18] and for gaseous intracavity absorption.[16] Note that for gaseous absorption the asymmetry is reversed in wavelength compared with a $LiNbO_3$ resonator. The absorption-induced heating lowered the crystal oven temperature required for optimum phase matching by approximately 1 deg and also induced thermal lensing in the resonator.[10] The complex interplay of these thermal phenomena requires an iterative process to maximize the 589-nm output power.

After careful system optimization an output power of 400 mW was measured for the primary beam, with the secondary beam containing an additional ≈15 mW. These beams have clean TEM_{00} modes with an aspect ratio near unity. No evidence of photorefractive damage was observed, corroborating earlier experience with pulsed and low-power cw sum-frequency generation of 589-nm radiation in congruent $LiNbO_3$.[2,19]

3. Comparison with Theory

To compare the experimentally observed sum-frequency power with theoretical expectations we use the theory of Boyd and Kleinman[20] (BK) to write the sum-frequency power P_3 as[21]

$$P_3 = \gamma_{SF} L_{\mathrm{pm}} P_1 P_2, \tag{1a}$$

where P_i are the beam powers in the nonlinear medium, L_{pm} is the phase-matched length, and γ_{SF} is the sum-frequency conversion factor with

$$\gamma_{SF} = \frac{4\omega_1\omega_2\omega_3 h}{\pi\varepsilon_0 c^4 n_3^{\,2}} d_{\mathrm{eff}}^{\,2}, \tag{1b}$$

where ω_i are the angular frequencies, n_i are the refractive indices of the crystal, d_{eff} is the effective nonlinear coefficient, ε_0 is the permittivity of vacuum, c is the speed of light in vacuum, and h is the dimensionless BK focusing factor.[20] The subscripts 1, 2, and 3 refer to the 1319-, 1064-, and 589-nm beams, respectively. Assuming zero absorption and no astigmatism, the BK focusing factor h can be written for our resonator as[20]

$$h(\xi) = \frac{1}{4\xi}\left|\int_{-\xi(1-\mu)}^{\xi(1+\mu)} \mathrm{d}\tau \,\frac{\exp(i\sigma_m\tau)}{1+i\tau}\right|, \tag{2a}$$

where the focusing parameter $\xi = L_{\mathrm{pm}}/(2z_R)$ is the ratio of the phase-matched length L_{pm} and the confocal parameter $2z_R$ and σ_m is the optimum phase-matching parameter, a function of ξ. The parameter μ describes the location of the resonator focus relative to that of the phase-matched portion of the resonator's beam path with

$$\mu(\alpha) = 1 - \frac{L_{\mathrm{rt}}}{L_{\mathrm{pm}}} = -(1 + 2\sin\alpha), \tag{2b}$$

where $\alpha = 6°$ is the angle between the phase-matched resonator leg and the resonator symmetry axis (see Fig. 2) resulting in $\mu(\alpha = 6°) = -1.21$. Figure 4 shows the calculated BK focusing factor h as a function of the focusing parameter ξ for both our resonator, i.e., $\mu(\alpha = 6°) = -1.21$, and the maximum for an isosceles triangular beam path with phase matching in one of the two equal-length legs, i.e., $\mu(\alpha \to 0°) = -1$. The Rayleigh length z_R can be calculated from the equation describing the curvature of a Gaussian beam:

$$R(z) = z\left[1 + \left(\frac{z_R}{z}\right)^2\right], \tag{3}$$

after setting z equal to the distance from the focus to the curved surface (i.e., $z = L_{\mathrm{rt}}/2$) and the radius $R(z)$ equal to the radius of the curved surface (i.e., $R = 28$ mm). This results in $z_R = 13.9$ mm, $\xi = 0.413$, and $h = 0.324$ as indicated in Fig. 4. Inserting this BK focusing factor h and the effective nonlinear coefficient of congruent lithium niobate[22] [i.e., $d_{\mathrm{eff}} = d_{31} = (5.77 \pm 0.71) \times 10^{-12}$ m/V] into Eq. 1(b) yields $\gamma_{\mathrm{SF}} = (0.31 \pm 0.08)\,(\mathrm{W\,m})^{-1}$. For the 11.5-mm-long phase-matched path this results in a sum-frequency power P_3 of

$$P_3 = \gamma P_1 P_2 = (0.0035 \pm 0.0009)\mathrm{W}^{-1} P_1 P_2. \tag{4}$$

By use of a similar notation as Ashkin *et al.*,[7] the intracavity powers P_i are described by a system of two equations ($i = 1, 2$):

$$P_i = \frac{1 - r_i}{(1 - \sqrt{r_i t_i})^2} P_{\mathrm{mi}}, \tag{5a}$$

where a lossless coating is assumed, P_{mi} is the mode-matched incident power, r_i is the power reflection coefficient of the crystal coating, and t_i is the round-trip power transmission coefficient of the crystal, all at the wavelength λ_i. The crystal transmission coefficient t_i can be written as the product of one factor that is due the inherent material extinction coefficient a_0 and one factor that is due to sum-frequency

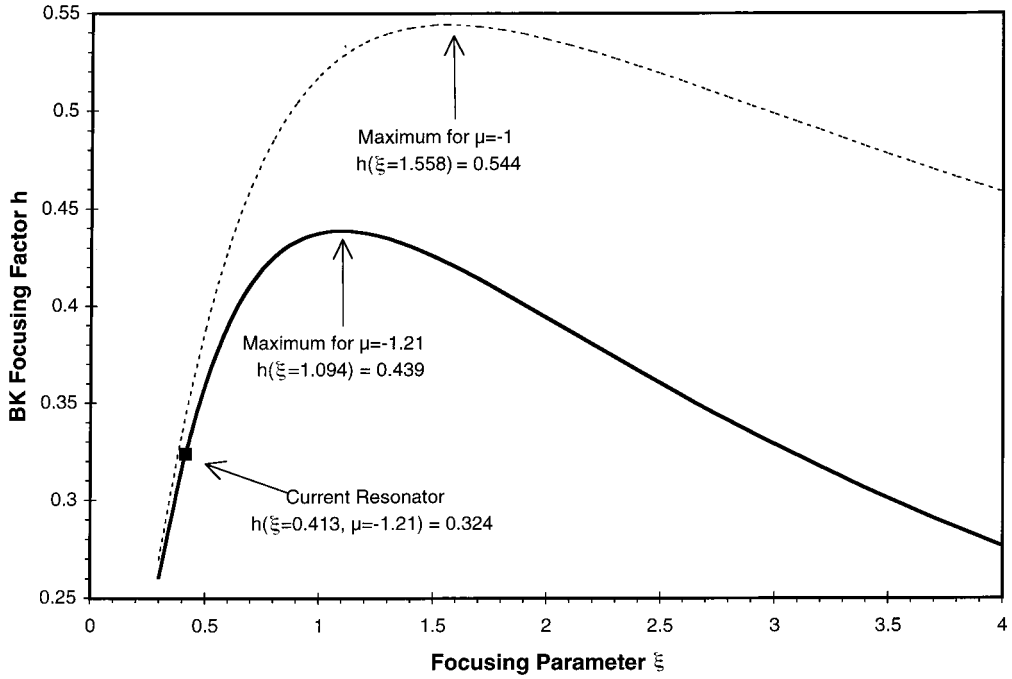

Fig. 4. Boyd and Kleinman (BK) focusing factor h as a function of the focusing parameter ξ for our resonator geometry (solid curve), our resonator (filled square), and the maximum for an isosceles triangular beam path with phase matching in one of the two equal-length legs (dashed curve).

conversion losses in the presence of the second infrared wavelength:

$$t_i = (1 - a_0 L_{rt})(1 - \gamma R_i P_j), \tag{5b}$$

where $j = 2$ for $i = 1$ and $j = 1$ for $i = 2$, and $R_i = \lambda_3/\lambda_i$ is the fraction of the sum-frequency power P_3 supplied by the field at wavelength λ_i. The intracavity powers P_i can be calculated by solving this system of two equations [Eqs. (5)]. As no analytical solution exists, numerical solutions were obtained.

The mode-matched laser powers were approximately $P_{m1} = 0.29$ W and $P_{m2} = 0.60$ W, and the extinction coefficient is $a_0 = (0.15 \pm 0.05)$ m^{-1} for congruent $LiNbO_3$ at our infrared laser wavelengths.[23] By use of these values and assuming impedance matching, Eqs. (5) yield calculated intracavity powers of $P_1 = 2.7$ W and $P_2 = 67$ W resulting in a calculated sum-frequency power of $P_3 = 0.62$ W inside the crystal. Impedance matching would require a crystal coating with a reflectivity of $r_1 = 89.2\%$ at 1319 nm and $r_2 = 99.1\%$ at 1064 nm. With the existing coatings ($r_1 = r_2 = 97\%$) the cavity is undercoupled at 1319 nm and overcoupled at 1064 nm. A calculation that uses the existing reflectivities and $\gamma = 0.0035$ W^{-1} yields calculated intracavity powers of $P_1 = 3.2$ W and $P_2 = 45$ W, resulting in a calculated sum-frequency power of $P_3 = 0.50$ W inside the crystal. However, the experimental output power was optimized by varying (among other things) the crystal temperature. This procedure optimizes the trade-off between single-pass conversion efficiency γ and impedance matching. Maximizing P_3 by varying γ numerically in Eqs. (5) yields a value (for our coating) of $\gamma_{opt} = 0.0018$ W^{-1}, resulting in calculated intracavity powers of $P_1 = 7.6$ W and $P_2 = 42$ W and a calculated sum-frequency power of $P_3 = 0.57$ W inside the crystal. At the 589-nm wavelength the extinction coefficient of lithium niobate is of the order of 2 m^{-1}, resulting in $\approx$4% transmission loss in addition to $\approx$4% reflection loss at the crystal coating.[23,24] For the optimum γ case, the calculated output power for the primary beam is therefore approximately 0.5 W, somewhat above the experimental measurement of 0.4 W. This slight disagreement is possibly due to the imperfect optimization of alignment, crystal temperature, etc. and also due to thermal lensing in the crystal.

4. Conclusions

We have demonstrated the generation of 400 mW of 589-nm cw radiation by sum-frequency generation in a monolithic lithium niobate resonator. Our system is all solid state, highly efficient, single frequency, and does not suffer from chaotic intensity fluctuations common for intracavity approaches. Current applications of this system include the generation of sodium D_2 resonance radiation for lidar probing of the mesopause region of the Earth's atmosphere.

It is a pleasure to acknowledge helpful discussions with Peter Bordui, Dave Gerstenberger, and Greg Mizell. We also thank one of the anonymous reviewers for valuable comments on the theoretical calculation. This research has been supported in part by the National Science Foundation grants ATM 9402166 and ATM 9612823.

References

1. H. M. Kretschmann, F. Heine, G. Huber, and T. Halldórsson, "All-solid-state continuous-wave doubly resonant all-intracavity sum-frequency mixer," Opt. Lett. **22,** 1461–1463 (1997).
2. H. Moosmüller and J. D. Vance, "Sum-frequency generation of continuous-wave sodium D_2 resonance radiation," Opt. Lett. **22,** 1135–1137 (1997).
3. C. Y. She, H. Latifi, J. R. Yu, R. J. Alvarez II, R. E. Bills, and C. S. Gardner, "Two-frequency lidar technique for mesospheric Na temperature measurements," Geophys. Res. Lett. **17,** 929–932 (1990).
4. C. Y. She and J. R. Yu, "Simultaneous three-frequency Na lidar measurements of radial wind and temperature in the mesopause region," Geophys. Res. Lett. **21,** 1771–1774 (1994).
5. W. R. Bosenberg, J. I. Alexander, L. E. Myers, and R. W. Wallace, "2.5-W, continuous-wave, 629-nm solid-state laser source," Opt. Lett. **23,** 207–209 (1998).
6. T. Baer, "Large-amplitude fluctuations due to longitudinal mode coupling in diode-pumped intracavity-doubled Nd:YAG lasers," J. Opt. Soc. Am. B **3,** 1175–1180 (1986).
7. A. Ashkin, G. D. Boyd, and J. M. Dziedzic, "Resonant optical second harmonic generation and mixing," IEEE J. Quantum Electron. **QE-2,** 109–124 (1966).
8. Y. Kaneda and S. Kubota, "Continuous-wave 355-nm laser source based on doubly resonant sum-frequency mixing in an external resonator," Opt. Lett. **20,** 2204–2206 (1995).
9. P. G. Wigley, Q. Zhang, E. Miesak, and G. J. Dixon, "High-power 467-nm passively locked signal-resonant sum-frequency laser," Opt. Lett. **20,** 2496–2498 (1995).
10. D. J. Berkeland, F. C. Cruz, and J. C. Berquist, "Sum-frequency generation of continuous-wave light at 194 nm," Appl. Opt. **36,** 4159–4162 (1997).
11. W. P. Risk and W. J. Kozlovsky, "Efficient generation of blue light by doubly resonant sum-frequency mixing in a monolithic KTP resonator," Opt. Lett. **17,** 707–709 (1992).
12. T. J. Kane and R. L. Byer, "Monolithic, unidirectional single-mode Nd-YAG laser," Opt. Lett. **10,** 65–67 (1985).
13. Lightwave Electronics, *Specifications of the Series 126 Diode-Pumped Non-Planar Ring Laser* (Lightwave Electronics, 1161 San Antonio Road, Mountain View, Calif. 94043, 1994).
14. G. J. Edwards and M. Lawrence, "A temperature-dependent dispersion equation for congruently grown lithium niobate," Opt. Quantum Electron. **16,** 373–375 (1984).
15. D. C. Gerstenberger, G. E. Tye, and R. W. Wallace, "Efficient second-harmonic conversion of cw single-frequency Nd:YAG laser light by frequency locking to a monolithic ring frequency doubler," Opt. Lett. **16,** 992–994 (1991).
16. P. Dubé, L.-S. Ma, J. Ye, P. Jungner, and J. L. Hall, "Thermally induced self-locking of an optical cavity by overtone absorption in acetylene gas," J. Opt. Soc. Am. B **13,** 2041–2054 (1996).
17. P. L. Hansen and P. Buchhave, "Thermal self-frequency locking of a doubly resonant optical parametric oscillator," Opt. Lett. **22,** 1074–1076 (1997).
18. K. An, B. A. Sones, C. Fang-Yen, R. R. Dasari, and M. S. Feld, "Optical bistability induced by mirror absorption: measurement of absorption coefficients at the sub-ppm level," Opt. Lett. **22,** 1433–1435 (1997).
19. T. H. Jeys, A. A. Brailove, and A. Mooradian, "Sum frequency generation of sodium resonance radiation," Appl. Opt. **28,** 2588–2591 (1989).
20. G. D. Boyd and D. A. Kleinman, "Parametric interaction of focused gaussian light beams," J. Appl. Phys. **39,** 3597–3639 (1968).
21. K. Sugiyama, J. Yoda, and T. Sakurai, "Generation of continuous-wave ultraviolet light by sum-frequency mixing of diode-laser and argon-ion-laser radiation in β-BaB_2O_4," Opt. Lett. **16,** 449–451 (1991).
22. M. M. Choy and R. L. Byer, "Accurate second-order susceptibility measurements of visible and infrared nonlinear crystals," Phys. Rev. B **14,** 1693–1706 (1976).
23. P. F. Bordui, Crystal Technology Inc., Palo Alto, Calif. 94303 (personal communication, 1994).
24. Y. C. See, S. Guha, and J. Falk, "Limits to the NEP of an intracavity $LiNbO_3$ upconverter," Appl. Opt. **19,** 1415–1418 (1980).